25th ABCM International Congress of Mechanical Engineering
October 20-25, 2019, Uberlândia, MG, Brazil

COB-2019-0820
MATHEMATICAL MODELLING OF A CANTILEVER BEAM DRIVEN BY TWO UNBALANCED ELECTRIC MOTORS

Arthur Mereles
Marcus Varanis
Anderson Silva
Federal University of Grande Dourados, R. João Rosa Góes, 1761 - Vila Progresso, Dourados - MS, 79825-070, Brazil.
arthur_guilherme_mereles@hotmail.com
marcusvaranis@ufgd.edu.br
andersonlangonesilva@hotmail.com

José Manoel Balthazar
Federal Technological University of Parana, Av. Monteiro Lobato, s/n - Jardim Carvalho, Ponta Grossa - PR, 84016-210, Brazil.
balthazar@utfpr.edu.br

Eduardo M. O. Lopes
Carlos Alberto Bavastri
Federal University of Parana, Rua XV de Novembro, 1299 - Centro, Curitiba - PR, 80060-000, Brazil
eduardo_lopes@ufpr.br
bavastri@ufpr.br

Abstract. *Non-ideal systems are seen in many situations where the dynamics of the system affects the energy source that drives it. In reality, every system is non-ideal at some degree and often the disregard of this fact can cause great discrepancies between the modelling and the test of the real system. In this manner, this work presents the modelling of a cantilever beam with two motors positioned on top of it. The motors are considered to be non-ideal energy sources and the beam is modeled as a continuous vibrating system. The goal of this work is to present a model in which some non-ideal phenomena can be predicted before the use of the real system in the field.*

Keywords: *non-ideal system, mathematical model, numerical simulations, continuous system.*

1. INTRODUCTION

One of the major challenges when it comes to engineering research is the study of systems with non-ideal energy sources, or non-ideal systems (Balthazar *et al.*, 2003). These systems are seen in many applications, where the power source gets affected by its interaction with the vibrating system. This causes many different phenomena that cannot be reached without the non-ideal consideration. Therefore, it is very important that such phenomena are well predicted before the system is used in practice, which requires a mathematical model that can predict these phenomena beforehand. References (Dimentberg, 1988; Evan-Iwanowski, 1976; Nayfeh and Mook, 2008) deal with non-ideal systems, and a more recent book is presented by Cveticanin *et al.* (2018).

An important phenomenon seen in many vibrating systems is the Sommerfeld effect, discovered in 1902 by Arnold Sommerfeld (Sommerfeld, 1902). This effect, also known as jump-phenomenon, happens when the power source is not capable of overcoming the natural frequency of the system. The source, which can be a motor, gets trapped in the resonance and is not able to reach the desired operation speed. The bigger problem, however, is that the amplitude of the vibrating system gets very high during this effect, which can be harmful for the structure. A great deal of studies have treated this phenomenon, such as (Samantaray *et al.*, 2010; Varanis *et al.*, 2018; Brasil and Balthazar, 2000; Piccirillo *et al.*, 2015).

Non-ideal systems often present a rich dynamics characteristics, which can be from periodic to chaotic. Due to their highly nonlinear characteristics, non-ideal systems are studied most of the times by numerical simulations, since an analytical approach is often not possible. References (Balthazar *et al.*, 2001; Wauer and Suherman, 1998) deal with the control of the Sommerfeld effect in vibrating systems. Some of the complex dynamics exhibited by non-ideals systems are explored by De Souza *et al.* (2005). Also, the attenuation of the jump-phenomenon is done by Piccirillo *et al.* (2014) and Felix *et al.* (2005), through magneto-rheological dampers and stick-slip friction and other non-linear energy sinks,

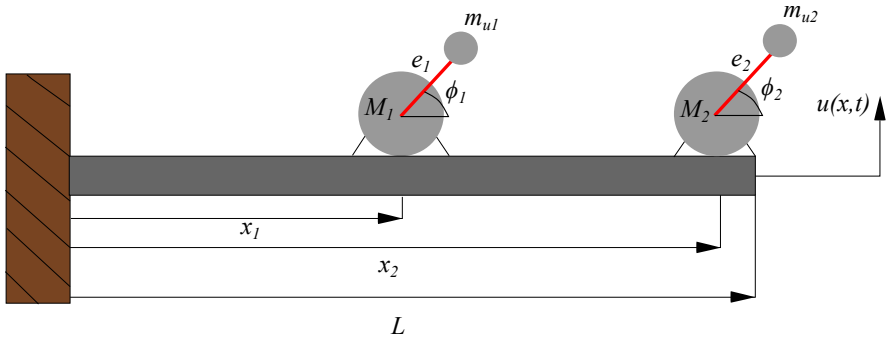

Figure 1: Depiction of the studied system.

respectively.

Most of the works cited above have studied the Sommerfeld effect in systems with one degree of freedom. Since most of the real structures used in engineering applications have many modes of vibration that are relevant for their dynamics, a multi degree of freedom approach is generally more accurate. Also, since the Sommerfeld effect occurs at a resonance state, by modeling a system with only one degree of freedom might not be enough to predict the phenomenon before the system is applied in the field.

Giving the aforementioned, this work presents a mathematical model of a cantilever beam with two electric motors positioned on top of it. The motors are considered to be non-ideal, which require two additional equations to the beam equation of motion. The responses of the system are obtained by means of numerical simulations and the results analyzed. Simulations performed at different work conditions showed to be possible to predict the Sommerfeld effect in the system.

2. MATHEMATICAL MODEL

The vibrating system consist in a cantilever beam with two unbalanced DC motors positioned on top of it, as depicted in Fig. 1. The motors are unbalanced by placing a mass m_{ui} at a distance of e_i, with $i = 1, 2$. The mass of the motors are denoted as M_i and are positioned at a distance x_i from the clamped end of the beam. The equation of motion of the beam, according to the Euler-Bernoulli theory, is given as

$$EI\frac{\partial^4 u}{\partial x^4}(x,t) + \left[m_b + \frac{M_1}{L}\delta(x-x_1) + \frac{M_2}{L}\delta(x-x_2)\right]\frac{\partial^2 u}{\partial t^2}(x,t) + c_v\frac{\partial u}{\partial t}(x,t) = \sum_{i=1}^{2}\frac{m_{ui}e_i}{L}\delta(x-x_i)[\ddot{\phi}_i(t)\cos\phi_i(t) - \dot{\phi}_i(t)^2\sin\phi_i(t)] \tag{1}$$

where E is the Young's modulus, I is the beam moment of area, $u(x,t)$ is the transverse displacement of the beam, m_b is the mass of the beam per unit length, δ is the Dirac delta, L is the length of the beam, c_v is the viscous damping coefficient, ϕ_i is the angular displacement of the motors and the dots represent time differentiation. As seen in Eq. (1), the motors are added directly in the equation of motion and not considered as boundary conditions. This approach makes the addition of several motors much easier.

Two additional equations are needed to describe the motors and their interaction with the vibrating system. The equations considered are (Kononenko, 1969; El-Badawy, 2007),

$$(I_i + m_{ui}e_i^2)\ddot{\phi}_i(t) = m_{ui}e_i\frac{\partial^2 u}{\partial t^2}(x_i,t)\cos\phi_i(t) + T_m(\dot{\phi}_i) \quad \text{for } i = 1, 2 \tag{2}$$

where I_i is the moment of inertia of the motors and T_m is the external torque, which depends on the motors' electric parameters. The relation of the torque considered is,

$$T_m(\dot{\phi}) = T_0\left(1 - \frac{\dot{\phi}(t)}{\Omega_{max}}\right) \tag{3}$$

where T_0 is the motor stall torque and Ω_{max} is the motor final speed. Equations (1) and (2) are nonlinear coupled partial differential equations. The equations can be solved by any discretization method, but, in this work, the modal expansion method is used, which states that,

$$u(x,t) = \sum_{n=1}^{\infty} W_n(x)U_n(t) \approx \sum_{n=1}^{N} W_n(x)U_n(t) \tag{4}$$

where N is the number of modes considered, and $W_n(x)$ and $U_n(t)$ are the mass normalized eigenfunction and the modal coordinate of the beam for the nth mode, respectively. By substituting Eq. (4) into Eqs. (1) and (2), and using the orthogonality conditions of the eigenfunctions, one may have,

$$\ddot{U}_n(t) + \sum_{k=1}^{N} c_{nk}\dot{U}_k(t) + \omega_n^2 U_n(t) = \sum_{i=1}^{2} \frac{m_{ui}e_i}{L} W_n(x_i)[\ddot{\phi}_i(t)\cos\phi_i(t) - \dot{\phi}_i(t)^2 \sin\phi_i(t)] \quad \text{for } n = 1, 2, ..., N \tag{5}$$

$$(I_i + m_{ui}e_i^2)\ddot{\phi}_i(t) = \sum_{n=1}^{N} m_{ui}e_i W_n(a_i)\ddot{U}_n(t)\cos\phi_i(t) + T_m(\dot{\phi}_i) \quad \text{for } i = 1, 2 \tag{6}$$

where ω_n is the nth beam natural frequency, and

$$c_{nk} = \frac{c_v}{m_b L}[\delta_{nk}L - M_1 W_k(x_1)W_n(x_1) - M_2 W_k(x_2)W_n(x_2)] \tag{7}$$

being δ_{nk} the Kronecker delta, which is zero for $n \neq k$ and unity for $n = k$. Equations (5) are the differential equation for the modal coordinates U_n and are coupled due to the non-proportional damping considered. Equations (6) are two scalar equations for the motors, and must be solved simultaneously with Eqs. (5).

2.1 Mode shapes and natural frequencies

The equation of motion for the free and undamped vibration of the beam is given as,

$$EI\frac{\partial^4 u}{\partial x^4}(x,t) + \left[m_b + \frac{M_1}{L}\delta(x - x_1) + \frac{M_2}{L}\delta(x - x_2)\right]\frac{\partial^2 u}{\partial t^2}(x,t) = 0 \tag{8}$$

considering the free vibration to be $u(x,t) = W(x)U(t) = W(x)A_0 e^{i\omega t}$, one may have,

$$EIW''''(x) - \left[m_b + \frac{M_1}{L}\delta(x - x_1) + \frac{M_2}{L}\delta(x - x_2)\right]W(x)\omega^2 = 0 \tag{9}$$

where the primes denotes differentiation with respect to x. Equation (9) has the following boundary conditions, which correspond to the clamped-free case,

$$W(0) = W'(0) = W''(L) = W'''(L) = 0 \tag{10}$$

Equation (9) can be solved using the Laplace Transform, which, using the boundary conditions, gives the following result,

$$\hat{W}(s) = \frac{M_1'\omega^2 W(x_1)e^{-sx_1} + M_2'\omega^2 W(x_2)e^{-sx_2} + W'''(0) + sW''(0)}{s^4 - \frac{\Omega^4}{L^4}} \tag{11}$$

where $M_i' = M_i/(EIL)$ and $\Omega^4 = \omega^2 m_b L^4/(EI)$. It is worth noting at this point that any other boundary conditions could be used with not much extra work needed to be done. To transform Eq. (11) back to the space domain, the Inverse Laplace Transform need to be used, which gives the following,

$$\begin{aligned} W(x) = {} & \frac{W'''(0)L^3}{2\Omega^3}\left(\sinh\frac{\Omega}{L}x - \sin\frac{\Omega}{L}x\right) + \frac{W''(0)L^2}{2\Omega^2}\left(\cosh\frac{\Omega}{L}x - \cos\frac{\Omega}{L}x\right) + \\ & \frac{W(x_1)M_1}{2m_b L}\frac{\Omega}{L}H(x - x_1)\left(\sinh\frac{\Omega}{L}(x - x_1) - \sin\frac{\Omega}{L}(x - x_1)\right) + \\ & \frac{W(x_2)M_2}{2m_b L}\frac{\Omega}{L}H(x - x_2)\left(\sinh\frac{\Omega}{L}(x - x_2) - \sin\frac{\Omega}{L}(x - x_2)\right) \end{aligned} \tag{12}$$

being H the Heaviside step function. Equation (12) has five unknown parameters: $W'''(0)$, $W''(0)$, $W(x_1)$, $W(x_2)$, and Ω. Since two boundary conditions were already used in the Laplace transform, that is $W(0) = 0$ and $W'(0) = 0$; two more equations are needed. These additional equations are the continuity of the function $W(x)$ at $x = x_1$ and $x = x_2$. Since there is four equations for five unknowns, one parameters is an arbitrary constant. By using the boundaries conditions and taking into account that $x_2 > x_1$, the mode shape function is obtained as,

$$W(x) = C_n\left[C_1(x) - \frac{C_2'''(L)}{C_1'''(L)}C_2(x)\right] \tag{13}$$

where C_n is an arbitrary constant and,

$$C_1(x) = K_1(x) + K_1(a_1)K_3(x) + [K_1(a_1)K_3(a_2) + K_1(a_2)]K_4(x) \tag{14}$$

$$C_2(x) = K_2(x) + K_2(a_1)K_3(x) + [K_2(a_1)K_3(a_2) + K_2(a_2)]K_4(x) \tag{15}$$

with,

$$K_1(x) = \frac{L^3}{2\Omega^3}\left(\sinh\frac{\Omega}{L}x - \sin\frac{\Omega}{L}x\right) \tag{16}$$

$$K_2(x) = \frac{L^2}{2\Omega^2}\left(\cosh\frac{\Omega}{L}x - \cos\frac{\Omega}{L}x\right) \tag{17}$$

$$K_3(x) = \frac{M_1}{2m_bL}\frac{\Omega}{L}H(x-a_1)\left(\sinh\frac{\Omega}{L}(x-a_1) - \sin\frac{\Omega}{L}(x-a_1)\right) \tag{18}$$

$$K_4(x) = \frac{M_2}{2m_bL}\frac{\Omega}{L}H(x-a_2)\left(\sinh\frac{\Omega}{L}(x-a_2) - \sin\frac{\Omega}{L}(x-a_2)\right) \tag{19}$$

The natural frequencies are obtained by the characteristic equation, which is given as,

$$C_1''(L)C_2'''(L) - C_2''(L)C_1'''(L) = 0 \tag{20}$$

after obtaining the eigenvalues Ω, the natural frequencies of the beam can be found using,

$$\omega = \Omega^2\sqrt{\frac{EI}{m_bL^4}} \tag{21}$$

The mode shapes given by Eq. (13) satisfy the following orthogonality conditions,

$$m_b\int_0^L W_m(x)W_n dx + \frac{M_1}{L}W_m(x_1)W_n(x_1) + \frac{M_2}{L}W_m(x_2)W_n(x_2) = \delta_{mn} \tag{22}$$

$$EI\int_0^L W_m''(x)W_n''(x)dx = \omega_n^2\delta_{mn} \tag{23}$$

which were used in the deduction of Eq. (5).

3. NUMERICAL SIMULATIONS

The following presents the results obtained by integrating the equations of motion. The equations were integrated using the variable step-size integrator *ode45* of the software Matlab. In addition, three modes of vibration were considered for the numerical simulations. The main parameters used are shown in Tab. 1 .

3.1 Mode shapes and natural frequencies

Before studying the forced vibration of the beam, the influence of the motors in its mode shapes and natural frequencies were analyzed. The results are shown in Fig. 2. This figure was obtained by varying the position of the center motor and maintaining the other one at the free end, thus $x_2 = L$. The case where the beam has no motors is also shown.

It is noted that the most dramatic changes are seen in the second and third mode shapes of the beam, Figures 2b and 2c. It is important to note the great discrepancies between the mode shapes with and without the motors, which are significant for the second and third modes, but not much for the first one. Also, the natural frequencies seem to increase as Motor 1 is positioned closer to the clamped end.

Table 1: Parameters used in the simulations

Parameter	Variable	Value
Beam mass per unit length	m_b	1.934 kg/m
Beam length	L	1 m
Young's Modulus	E	200 GPa
Beam area moment of inertia	I	482.96 mm^4
Viscous damping coefficient	c_v	0.1 Nm/s
Mass of motors	M_1 and M_2	3.87 kg
Moment of Inertia of motors	I_1 and I_2	0.021 kgm^2
Unbalance of motors	$m_{u1}e_1$ and $m_{u2}e_2$	0.02 kgm

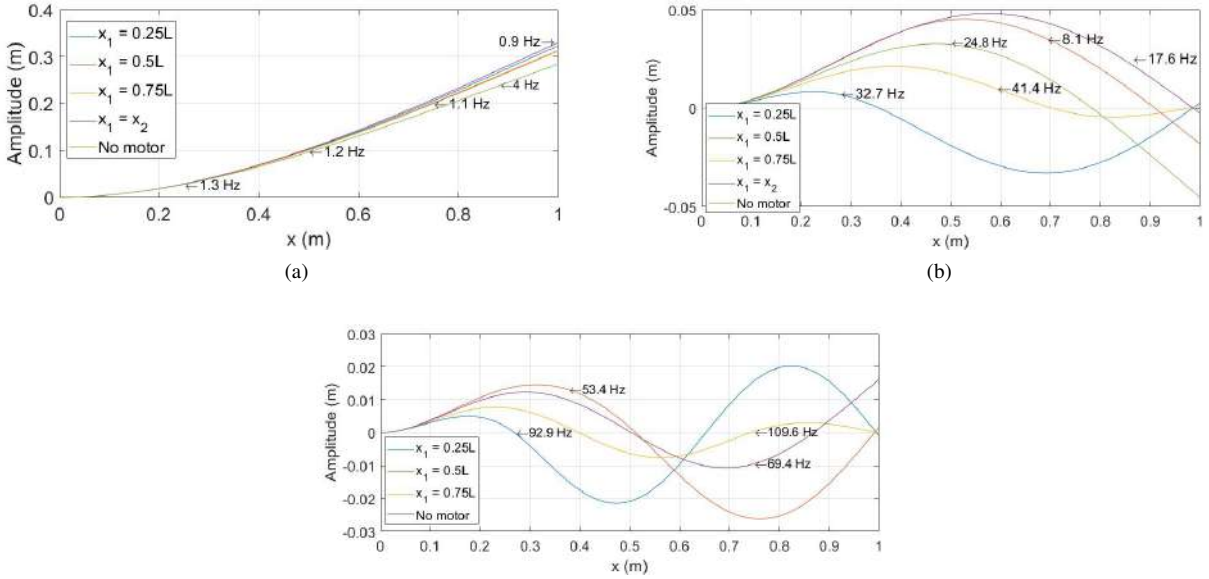

(a) (b)

(c)

Figure 2: Influence of the position of Motor 1 in the mode shapes and natural frequencies of the beam: (a) First mode, (b) Second mode and (c) Third mode.

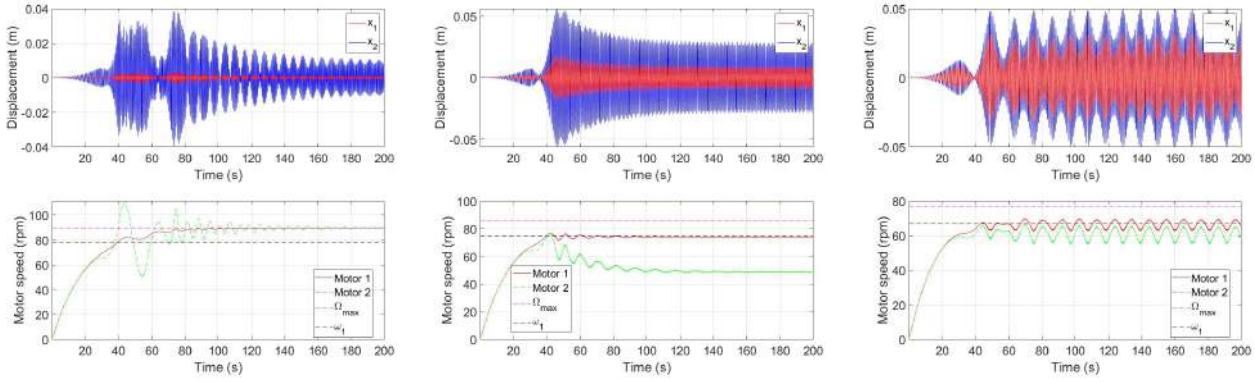

(a) (b) (c)

Figure 3: Results for crossing the first natural frequency considering $T_0 = 0.01$ Nm and $x_2 = L$: (a) $x_1 = 0.25L$, (b) $x_1 = 0.5L$, (c) $x_1 = 0.75L$.

3.2 Influence of the position of the motors

In the first analysis performed in the system, the position of the motors was varied and they were set to cross the natural frequencies of the beam. Since varying the motors' positions also vary the beam natural frequencies, all speeds were set to 15 % higher than the natural frequency of the mode studied, i.e., $\Omega_{max} = 1.15\omega_n$. Thus, for each motors configuration, the final speed was different, but the proportionality with the natural frequency was the same. Figure 2 shows the values of the natural frequencies for the configurations used. The stall torque was set so that the Sommerfeld effect could be seen. Also, analysis were performed by crossing the three firsts natural frequencies.

Figure 3 shows the results for crossing the first natural frequency. The upper figures presents the displacements and the bottom ones the corresponding motor speed. It is noted that the response of the system varies greatly when one of the motors is positioned in a different location. Only when Motor 1 was positioned at a quarter from the clamped end, Figure 3a, that the motors achieved their given max velocities. When Motor 1 was at the center and at a quarter from the free end, Figures 3b and 3c, the speed of the motors did not cross the natural frequency and the displacement of the beam was greatly increased, which is a characteristic of the Sommerfeld effect. It is interesting to note that when $x_1 = 0.5L$, the motor positioned at the free end, Motor 2, stayed in a speed lower than the first natural frequency. With a higher stall torque, the motors cross easily the first natural frequency. These results show, however, that even with a very small torque, the operation speed of the motors can be achieved, provided they are correctly positioned on the beam.

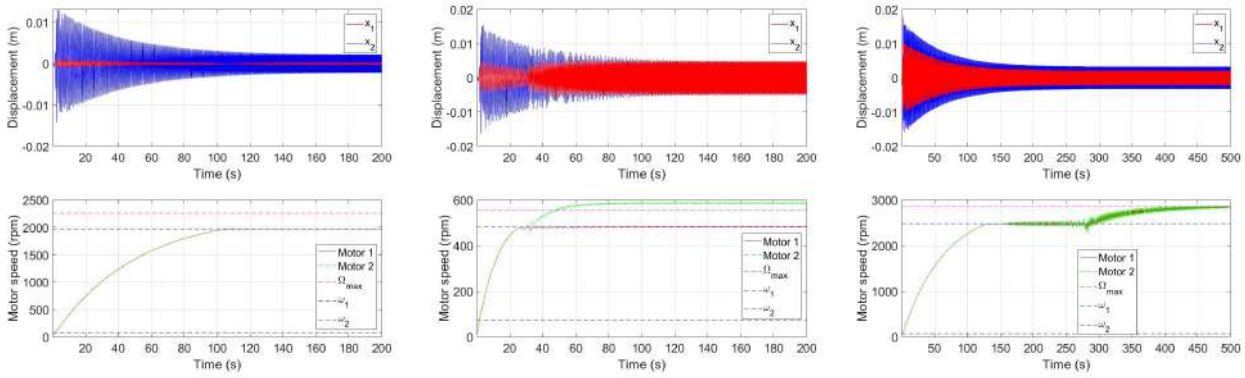

(a) (b) (c)

Figure 4: Results for crossing the second natural frequency considering $T_0 = 0.1$ Nm and $x_2 = L$: (a) $x_1 = 0.25L$, (b) $x_1 = 0.5L$, (c) $x_1 = 0.75L$.

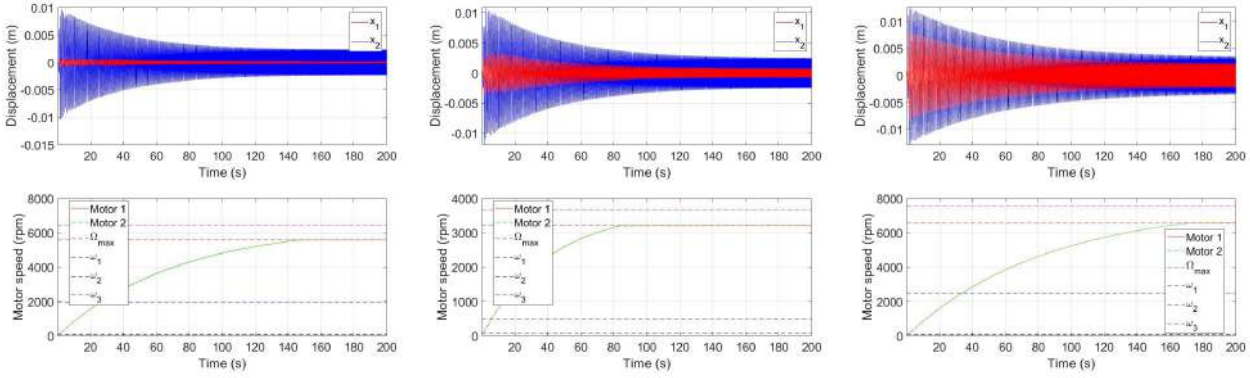

(a) (b) (c)

Figure 5: Results for crossing the third natural frequency considering $T_0 = 0.2$ Nm and $x_2 = L$: (a) $x_1 = 0.25L$, (b) $x_1 = 0.5L$, (c) $x_1 = 0.75L$.

Figure 4 presents the case when the motors were set to cross the second natural frequency of the beam. In this case, the response of the system was even more varied with the different motors locations. In the case with Motor 1 at a quarter from the clamped end, Figure 4a, neither of motors were able to cross the second natural frequency. As for the case when Motor 1 was at the mid-span, Figure 4b, only Motor 2 crossed the natural frequency. This happened mainly due to the second mode shape, which has a higher amplitude near the mid-span then at the free end, as one can note from Fig. 2b. When Motor 1 was at a quarter from the free end, Figure 4c, both motors achieved the operation speed, though with a little difficulty. This case presented a different result from Fig. 4b because Motor 1 is close to a node point.

In the last case, the motors were set to cross the third natural frequency, as shown in Fig. 5. The results were very similar for all motors configurations, since in all cases the motors were not able to cross the third natural frequency. The difference was only when the motors got stuck, and the amplitude of position x_2, which was different according to the differences in the third mode shapes (Figure 2c).

3.3 Influence of the motors' parameters

In this study, the stall torque of both motors were considered to be different. Only the case with the motors at the mid-span and at the free end, that is $x_1 = 0.5L$ and $x_2 = L$, was considered. Also, the analysis was performed for the crossing of the first and second natural frequencies only.

Figure 6 shows the results for the same configuration as Fig. 3b but with a higher stall torque. The figure presents two different cases: in Fig. 6a both motors have the same torque, $T_{01} = T_{02} = 0.5$; and in Fig. 6b Motor 1 and 2 have torques of $T_{01} = 0.1$ Nm and $T_{02} = 0.5$ Nm, respectively. It is interesting to note that when both motors have the same high torque, the amplitude of the beam stays high, and the speed of the motors oscillate a great amount. When the motor at the mid-span has less torque than the one at the free end, the amplitude stays low and the motors oscillate very little around the operation speed. This result shows that by knowing the interaction of the motors with the structure, less powerful

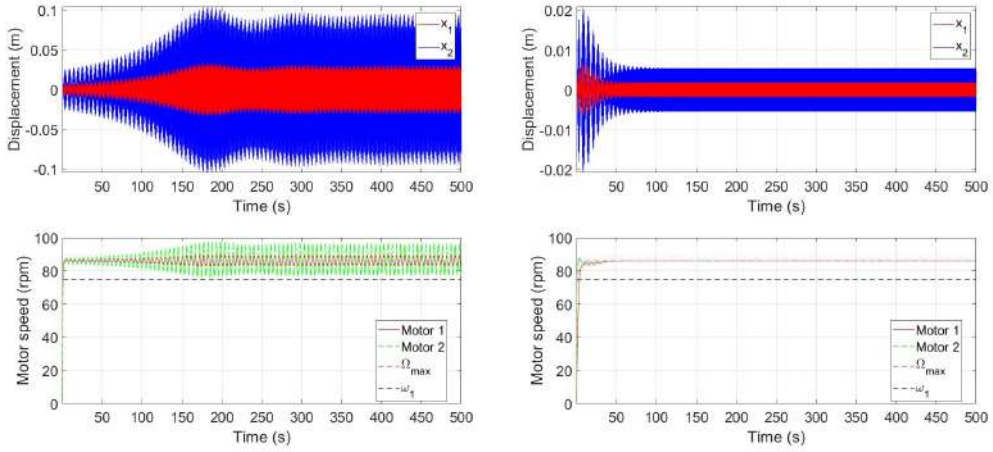

(a) (b)

Figure 6: Results for different stall torques for the motors in the passage through the first natural frequency with $x_1 = 0.5L$ and $x_2 = L$: (a) $T_{01} = T_{02} = 0.5$ Nm and (b) $T_{01} = 0.1$ Nm and $T_{02} = 0.5$ Nm.

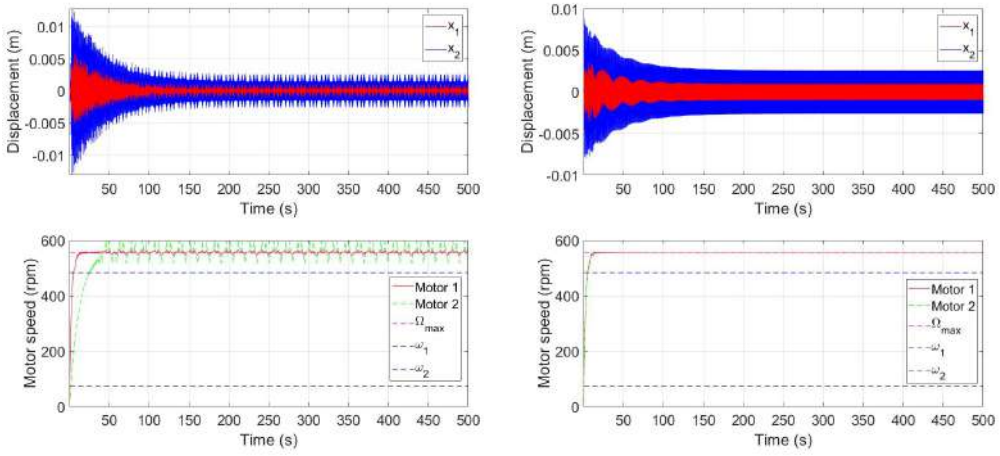

(a) (b)

Figure 7: Results for different stall torques for the motors in the passage through the second natural frequency with $x_1 = 0.5L$ and $x_2 = L$: (a) $T_{01} = 0.5$ Nm and $T_{02} = 0.1$ Nm and (b) $T_{01} = T_{02} = 0.5$ Nm.

motors can be chosen depending on their locations on the structure.

Another analysis performed is shown in Fig. 7. Similar to what was done before, two cases were studied: in Fig. 7b both motors have the same torque, $T_{01} = T_{02} = 0.5$; and in Fig. 7a Motor 1 and 2 have torques of $T_{01} = 0.5$ Nm and $T_{02} = 0.1$ Nm, respectively. From these results, it is seen that the case where both motors have the same high torque is better, since when Motor 2 have a lower torque the speed of the motors oscillate a great amount. Despite of this, the amplitude in both cases was fairly similar, with a difference in the harmonics of the motors in Fig. 7a, which excite the beam as well. These results show that the knowledge of the mode shape of the structure in which the motors will excite the most is fundamental for their proper operation.

3.4 Influence of external damping

The aim of the last analysis performed was studying the effect of the external damping in the occurrence of the Sommerfeld effect. It was mainly to see if the motors could cross the natural frequencies with a higher damping. Only the case with Motor 1 at the mid-span and Motor 2 at the free end was considered, thus $x_1 = 0.5L$ and $x_2 = L$. The results are presented in Fig. 8. These responses are for the same cases as Figs. 3b, 4b and 5b; but with a coefficient of damping of $c_v = 1$ Nm/s, which is ten times higher than the value considered before, shown in Table 1. By comparing the cases with high damping with their corresponding cases with low damping, one can note that the Sommerfeld still occurs

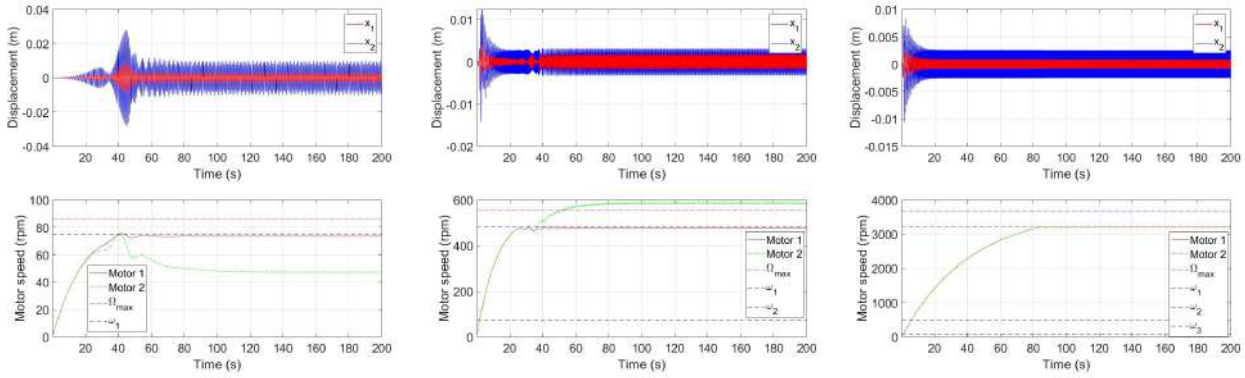

(a) (b) (c)

Figure 8: Results for crossing the natural frequencies considering $c_v = 1$ Nm/s, $x_1 = 0.5L$ and $x_2 = L$: (a) $T_0 = 0.01$ Nm, (b) $T_0 = 0.1$ Nm, (c) $T_0 = 0.2$ Nm.

in all cases. The damping has the effect of only decreasing the amplitude of the beam and the oscillation of the speed of the motors. A major difference is seen in the second natural frequency, Figure 8b, which showed the amplitude at the mid-span to be less than the one at the free end. This result was not seen when a low damping is considered, as one can note in Fig. 4b, where the exact opposite occured. With these results one can conclude that, once the Sommerfeld effect occurs, the only way to avoid it is to enhance the power capability of the motors; otherwise they will not be able to reach their operating speed.

4. CONCLUSIONS

This work presented a continuous vibrating model of a beam with two non-ideal motors positioned on top of it. The model allows the motors to be positioned anywhere over the beam, which, as shown, influence its mode shapes and natural frequencies. The results showed that the knowledge of the mode shapes are very important in the proper operation of the motors. In addition, the analysis performed focused in studying when the Sommerfeld effect can occur with motors of different characteristics and positioned at varied locations over the beam.

Three separate studies were performed through numerical simulations. In the first one the influence in the locations of the motors in the occurrence of the Sommerfeld effect was seen. Given the results shown, it can be concluded that the location of the motors greatly affects the dynamics of the system. Also, it was shown that, depending on the motors positions, they can cross the natural frequencies of the beam with low values of torques, which means a less powerful energy source is needed for the proper operation of the motors.

In the two following studies, the influence in the motors parameters and the external damping were seen through the simulations. The results showed that, in some cases, is better to have one motor with higher torque than the other. This, however, depends mainly on the most excited mode shape of the structure, which is the closest to the operating speed of the motors. The external damping was shown to have little effect in the dynamics of the system, and the increase in the damping of the system is not enough to avoid the resonance capture.

5. REFERENCES

Balthazar, J.M., Cheshankov, B.I., Ruschev, D., Barbanti, L. and Weber, H., 2001. "Remarks on the passage through resonance of a vibrating system with two degrees of freedom, excited by a non-ideal energy source". *Journal of Sound and Vibration*, Vol. 239, No. 5, pp. 1075–1085.

Balthazar, J.M., Mook, D.T., Weber, H.I., Brasil, R.M., Fenili, A., Belato, D. and Felix, J., 2003. "An overview on non-ideal vibrations". *Meccanica*, Vol. 38, No. 6, pp. 613–621.

Brasil, R. and Balthazar, J.M., 2000. "Nonlinear oscillations of a portal frame structure excited by a nonideal motor". In *Control of Oscillations and Chaos, 2000. Proceedings. 2000 2nd International Conference*. IEEE, Vol. 2, pp. 275–278.

Cveticanin, L., Zukovic, M. and Balthazar, J.M., 2018. *Dynamics of mechanical systems with non-ideal excitation*. Springer.

De Souza, S., Caldas, I.L., Viana, R., Balthazar, J.M. and Brasil, R., 2005. "Impact dampers for controlling chaos in systems with limited power supply". *Journal of Sound and Vibration*, Vol. 279, No. 3-5, pp. 955–967.

Dimentberg, M.F., 1988. *Statistical dynamics of nonlinear and time-varying systems*, Vol. 5. Research Studies Press.

El-Badawy, A.A., 2007. "Behavioral investigation of a nonlinear nonideal vibrating system". *Journal of Vibration and Control*, Vol. 13, No. 2, pp. 203–217.

Evan-Iwanowski, R., 1976. *Resonance oscillations in mechanical systems*. North-Holland.

Felix, J.L., Balthazar, J.M. and Brasil, R.M., 2005. "On tuned liquid column dampers mounted on a structural frame under a non-ideal excitation". *Journal of Sound Vibration*, Vol. 282, pp. 1285–1292.

Kononenko, V.O., 1969. *Vibrating systems with a limited power supply*. Iliffe.

Nayfeh, A.H. and Mook, D.T., 2008. *Nonlinear oscillations*. John Wiley & Sons.

Piccirillo, V., Balthazar, J., Tusset, A., Bernardini, D. and Rega, G., 2015. "Non-linear dynamics of a thermomechanical pseudoelastic oscillator excited by non-ideal energy sources". *International Journal of Non-Linear Mechanics*, Vol. 77, pp. 12–27.

Piccirillo, V., Tusset, A.M. and Balthazar, J.M., 2014. "Dynamical jump attenuation in a non-ideal system through a magnetorheological damper". *Journal of Theoretical and Applied Mechanics*, Vol. 52, No. 3, pp. 595–604.

Samantaray, A., Dasgupta, S. and Bhattacharyya, R., 2010. "Sommerfeld effect in rotationally symmetric planar dynamical systems". *International Journal of Engineering Science*, Vol. 48, No. 1, pp. 21–36.

Sommerfeld, A., 1902. "Beiträge zum dynamischen ausbau der festigkeitslehe". *Physikal Zeitschr*, Vol. 3, pp. 266–286.

Varanis, M., Balthazar, J., Silva, A., Mereles, A. and Pederiva, R., 2018. "Remarks on the sommerfeld effect characterization in the wavelet domain". *Journal of Vibration and Control*, p. 1077546318771804.

Wauer, J. and Suherman, S., 1998. "Vibration suppression of rotating shafts passing through resonances by switching shaft stiffness". *Journal of vibration and acoustics*, Vol. 120, No. 1, pp. 170–180.

6. RESPONSIBILITY NOTICE

The authors are the only responsible for the printed material included in this paper.